Santamarina, J.C. and Cho, G.C. (2004), Soil Behavior: The Role of Particle Shape, Proc. Skempton Conf., March, London.

# Soil behaviour: The role of particle shape

**J.C. Santamarina**, Georgia Tech, Atlanta, USA
**G.C. Cho**, KAIST, Daejeon, South Korea

## Abstract
This manuscript reviews particle shape, its development in fine-grained soils (particle size D<~10μm) and coarse-grained soils (D>~100μm), shape characterization, and the role of particle shape on fabric formation and macroscale soil properties. Shape-dependent microscale mechanisms are hypothesized to explain previously published studies as well as new soil behaviour data. Particle shape emerges as a significant parameter that needs to be properly characterized and documented.

## Introduction
Soils are made of mineral grains. The grain size distribution of a soil (mean size $D_{50}$ and range $C_u$) determines the governing particle-level forces, inter-particle packing and the ensuing macroscale behaviour; therefore, grain size distribution plays a central role in soil classification systems. On the other hand, there is an increased realization of the relevance of particle shape in soil behaviour and in other particulate materials such as pavements, mining products, food grains, and pharmaceutical particles.

Grain shape is established at three different scales: the global form, the scale of major surface features and the scale of surface roughness. Each scale reflects aspects of the formation history, and participates in determining the global behaviour of the soil mass, from particle packing to mechanical response. This manuscript presents a broad review of particle shape and its relevance on soil behaviour, including a discussion of underlying micromechanical processes and measured macroscale results.

## Grain formation: The origin of particle shape
Particle size and shape reflect material composition, grain formation and release from the mineral matrix, transportation, and depositional environments. The most relevant processes involved in the formation of small (particle size D<~10μm) and large mineral grains (D>~100μm) are discussed next.

### Small grains (Chemical and biological effects)
Clay minerals result from weathering in aqueous environments (typically by dissolution of various minerals), and evolve in response to the chemical and thermal local conditions (Velde 1992). The size and shape of particles from solution are determined by a combination of:

- Crystallographic structure e.g., hexagonal shape of kaolinite particles (Figure 1-a) versus the tubular shape of halloysite.
- Interfacial energy between the precipitate and the matrix (proportional to surface area).
- Elastic strain energy from lattice accommodation across the interface (proportional to the particle volume - Nabarro 1940).

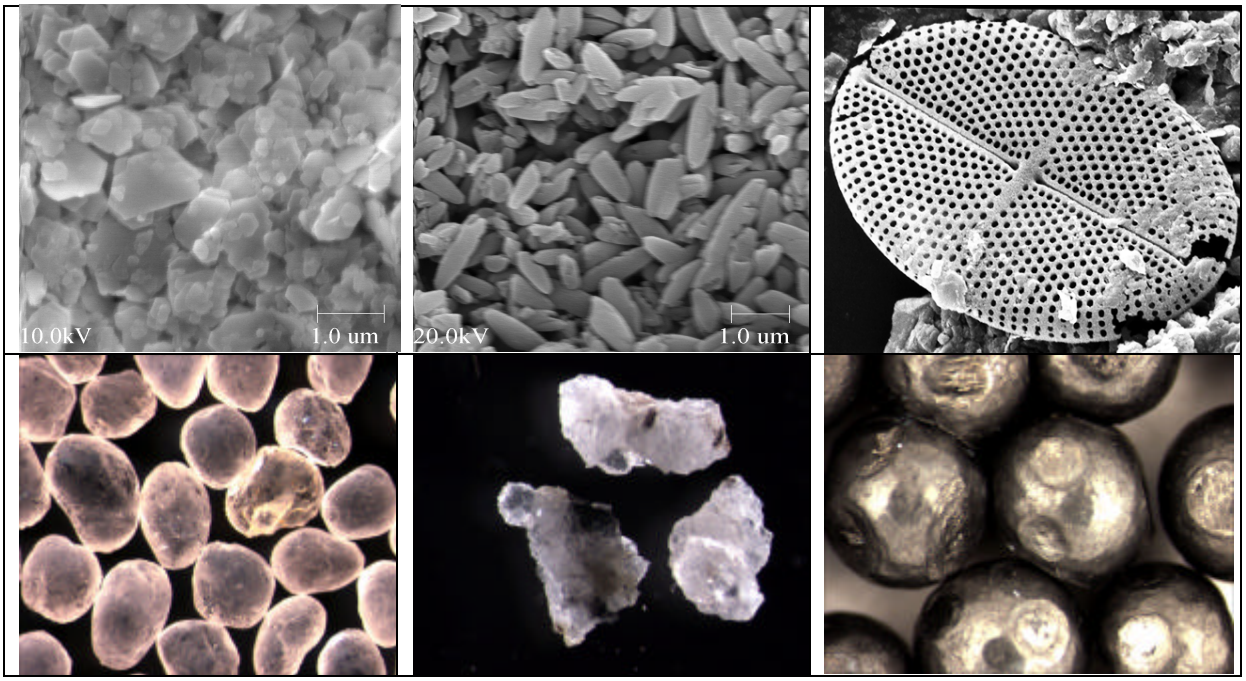


Figure 1. The shape of grains. Small grains - μm size: (a) kaolinite, (b) precipitated calcium carbonate, (c) diatom (University College London). Large grains - mm size: (d) Ottawa sand, (e) crushed sand, (f) preloaded lead shot (simulates locked sands).

- Externally applied stress -such as interacting particles- which alters the particle crystallographic structure and adds a mismatch at the interface with the precipitating phase (Li and Chen 1999). When the particle is elastically heterogeneous, an applied stress causes further changes in the crystal structure and alters particle growth.
- Diffusion or advection-controlled mass transfer required for particle growth (e.g., precipitated $CaCO_3$). Diffusion-controlled mass transfer becomes unstable after a certain particle size. On the other hand, the particle grows faster on the surface towards the incoming flow in advection-controlled mass transfer (Noh et al. 1998). Figure 1-b shows the elongated shape of precipitated calcium carbonate.
- The presence of impurities or dopants that limit crystal growth (review in Rahaman 1995).

The varied morphology of clay minerals, their associated particle size, and the growth of large particles at the expense of smaller ones -Ostwald ripening- reflect the interplay among these mechanisms (e.g., well-crystallized kaolinite).

*Microfossils*. Diatoms, radiolarian, and foraminiferan among others, are siliceous or carbonate "grains" secreted by organisms in fresh water or marine environments. The size of microfossils ranges from sub-micron to 500 μm. Their shape often involves exceptional geometric designs, high porosity and surface roughness (Figure 1-c). Soils with microfossils frequently exhibit unique behaviour (e.g., diatomaceous soils, Mexico City clay, Ariake clay).

## Large grains (Mechanical effects)

The size and shape of coarse grains, such as quartz grains, is strongly affected by the conditions when quartz solidifies in igneous rocks (Smalley 1966). Once a grain is released, the evolution of shape and surface features reflects mechanical and chemical effects. The transition region from chemical to mechanically controlled shape occurs between particles that are ~50μm to ~400μm. The probability of chemical effects and abrasion increases with age, and older sands tend to be rounder regardless of particle size (e.g., Figures 1-d vs. 1-e).

*General shape.* The larger the particle the higher the probability of imperfections and brittle fracturing (typically in grain size >400μ). Conversely, smaller particles are stronger by lack of imperfections, then, failure by cleavage along crystal atomic planes becomes energetically advantageous and the resulting particles are more platy (Margolis and Krinsley 1974). High-coordination conditions (rather than a diametrically loaded isolated particle) promotes the splitting of elongated particles (i.e., increased cubicity) and shear abrasion.

*Roundness and roughness*. Impact-based abrasion is related to kinetic energy (size, density, velocity), strength, and stress concentration which is higher in more angular particles; therefore roundness is the asymptotic shape of abrasion. The smaller a particle is, the smaller its mechanical momentum and the lower the probability of mechanically induced surface features. Eolian abrasion becomes ineffective for quartz particles smaller than ~50μm. Aqueous abrasion is less efficient because of viscous losses when the two particles approach each other, and it becomes ineffective for particles smaller than ~500μm (Kuenen 1960). On the other hand, the smaller the particle, the higher its chemical reactivity and the probability of chemically controlled surface features. The surface of large particles often exhibits a disrupted layer (thickness up ~1% the particle diameter) which could be chemically more reactive than amorphous silica and sustain solution-precipitation (Margolis and Krinsley 1974).

*After soil formation*. The shape of grains evolves by mechanisms such as pressure solution-precipitation (diffusion), contact yield and viscous flow or sintering (Rahaman 1995). Locked sands are a salient natural example (Dusseault and Morgenstern 1979). Figure 1-f shows the final shape of lead shot after loading a random packing to a low final porosity (n~0.15).

## Shape Description and Measurement

Particle shape irregularity manifests at three main scales (Figure 2-a; Wadell 1932, Krumbein 1941, Powers 1953, Krumbein and Sloss 1963, Barrett 1980): *sphericity* S rather than ellipticity or platiness, *roundness* R versus angularity, and *smoothness* in opposition to roughness. Sphericity is quantified as the diameter ratio between the largest inscribed and the smallest circumscribing sphere. Roundness is quantified as the average radius of curvature of surface features relative to the radius of the maximum sphere that can be inscribed in the particle. Figure 2-b shows particles with different sphericity and roundness. Roughness relates to surface features much smaller than the particle diameter.

*Sphericity and roundness* can be estimated by visual comparison with charts, such as the one shown in Figure 2-b (Folk 1955, Barrett 1980). Differences in estimated roundness and sphericity by different assessors is in the order of 0.1 and does not exceed 0.2. Digital image analysis facilitates the systematic evaluation of mathematical descriptors of particle shape including Fourier analysis, fractal analysis and other hybrid techniques (e.g., Meloy 1977, Clark 1987, Hyslip and Vallejo 1997, Bowman et al. 2001).

The direct measurement of *roughness* is cumbersome: the fractal nature of rough surfaces implies lack of characteristic scale. Therefore, the relevant observation length of roughness becomes the interparticle contact area: this is a particle's link to its neighbour.

Finally, shape parameters can be inferred from macro-scale behaviour of the soil mass. For instance, particle shape affects granular flow on inclined planes, residence time on sieves, and sedimentation time in a fluid column. However, separating the relative contributions of roughness, sphericity and roundness may not be possible from single microscale tests.

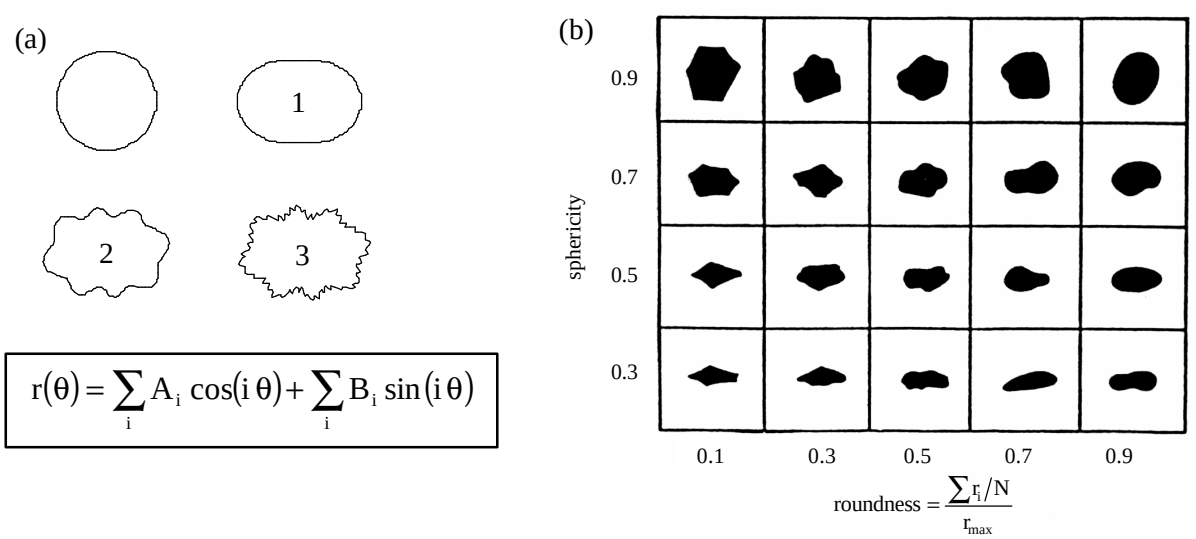


Figure 2. Scales in particle shape irregularity. (a) #1 ellipticity vs. sphericity [low harmonics i~1]; #2 angularity vs. roundness [i~10]; and #3 roughness vs. smoothness [i~100]. (b) Particles with different sphericity and roundness (from Krumbein and Sloss 1963)

## Specific Surface and Plasticity

The specific surface $S_a$ of a particle is the ratio between its surface area and mass. It follows from simple geometric considerations that the specific surface is proportional to the inverse of the smallest particle dimension $L_{min}$,

$$S_a = \frac{c}{L_{min} \rho_w G_s} \qquad (1)$$

where Gs is the specific gravity of the particle mineral, ρw=1 g/cm3 is the mass density of water, and the parameter c=6 for spherical and cubical particles, c=4 for prismatic and cylindrical particles, and c=2 for platy particles. Therefore, grain size distribution and specific surface measurements can be used to infer shape.

The relevance of particle shape on specific surface implies a direct link to plasticity. Consider the following examples (sensible values are listed): *montmorillonite*: $S_a$=800 $m^2$/g, LL= 700; *attapulgite*: $S_a$≈160 $m^2$/g, LL= 220; *illite*: $S_a$=90 $m^2$/g, LL= 80; *kaolinite*: $S_a$=10 $m^2$/g, LL= 40; *silt and sand*: $S_a$<0.1 $m^2$/g, LL= n/a.

## Fabric - Terminal densities - Anisotropy

The relative arrangement of particles depends on interparticle forces and particle shape: small particles (d< ~10μ) are mostly platy and packing is controlled by electrical forces, while large particles (d> ~100μ) tend to be bulky and packing is determined by gravitational forces.

### Fabric in fine-grained soils

The charge on mineral surfaces and edges depends on the ionic concentration and pH of the surrounding fluid, and is compensated by the counterion cloud that surrounds the particle. The resulting electrical interparticle forces include Coulombian attraction between positively charged edges and negatively charged faces, double layer repulsion, and van der Waals attraction. The first two depend on ionic concentration and pH, while van der Waals does not. Then, the following particle arrangements can be identified:

- dispersed: pore fluid with low ionic concentration and pH away from the mineral's self-buffering pH (double layer repulsion prevents particle association).

- edge-to-face (EF): when the pH is between isoelectric points so that edges and faces have different charge. Particles must be thick so that the face double layer does not hide the edge charge (e.g., kaolinite), otherwise EF flocculation is not observed (e.g., montmorillonite - Rand et al. 1980, Chen et al. 1990).
- face-to-face (FF): when van der Waals attraction prevails at high ionic concentration.
- edge-to-edge (EE): Intermediate condition between EF flocculation and FF aggregation.

A general fabric map in the c-pH space is presented in Figure 3-a.

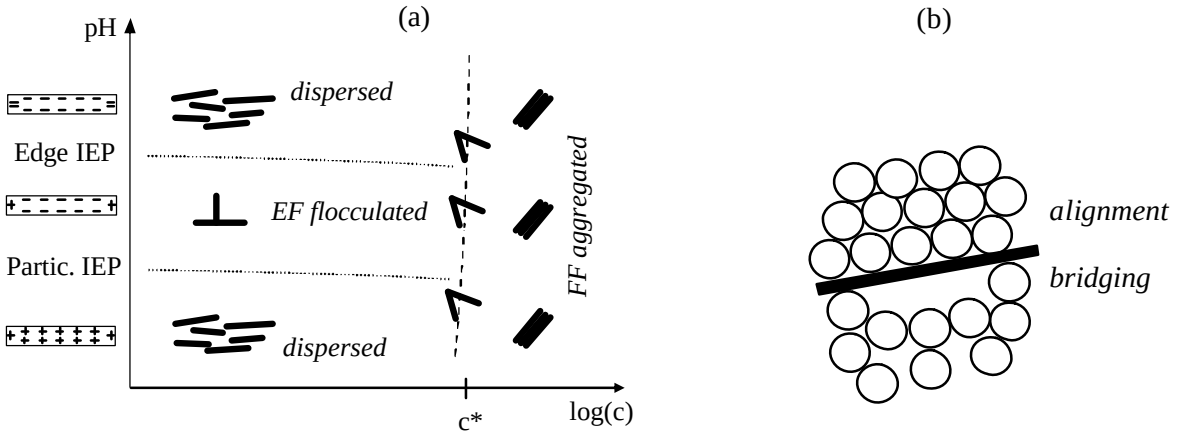


Figure 3. Platy particles. (a) General fabric map. (b) Platy and round particles: alignment and bridging.

## Fabric in coarse-grained soils

The loosest stable packing that can be obtained in mono-sized spheres is the simple cubic packing (CN=6, e=0.91, n=0.48), and the densest packing is the tetrahedral or pyramidal packing (CN=12, e=0.34, n=0.26). Particle shape affects attainable void ratios. In particular, the maximum and minimum void ratios increase with decreased roundness or sphericity (Fraser 1935, Shimobe and Moroto 1995, Miura et al. 1998, Cubrinovski and Ishihara 2002). Expressions from $C_u$=1 follow (Youd 1973):

$$e_{max} = 0.554 + 0.154R^{-1} \qquad e_{min} = 0.359 + 0.082R^{-1} \qquad (2)$$

The difference between extreme void ratios $e_{max}$-$e_{min}$ also increases as particles become angular and non-spherical. Results from a particle level analysis are shown in Figure 4-a, for simple cubic and tetrahedral packings as the geometry is stretched and particles become either rod-like or platy. Data in Figure 4-b are gathered with natural and crushed sands.

Settling coarse particles (that is, when the particle self weight is important in comparison to electrical inter-particle forces) come to rest with their longest axis in the horizontal position to attain the lowest potential energy. Therefore, *non-spherical platy or ellipsoidal particles* with slenderness as low as ~1.1 favour the development of inherent fabric anisotropy (Rothenburg 1993).

## Mixtures of platy and round particles

The presence of a flat surface enforces order in the packing of round particles that fall on top (Figure 3-b). Ordering typically extends for 5-to-10 particle diameters away from the flat surface. On the other hand, a free falling platy particle tends to settle on a horizontal position. If its size is larger than the diameter of round particles, then the flat particle will bridge over round particles leaving a high local porosity underneath. Ordering and bridging

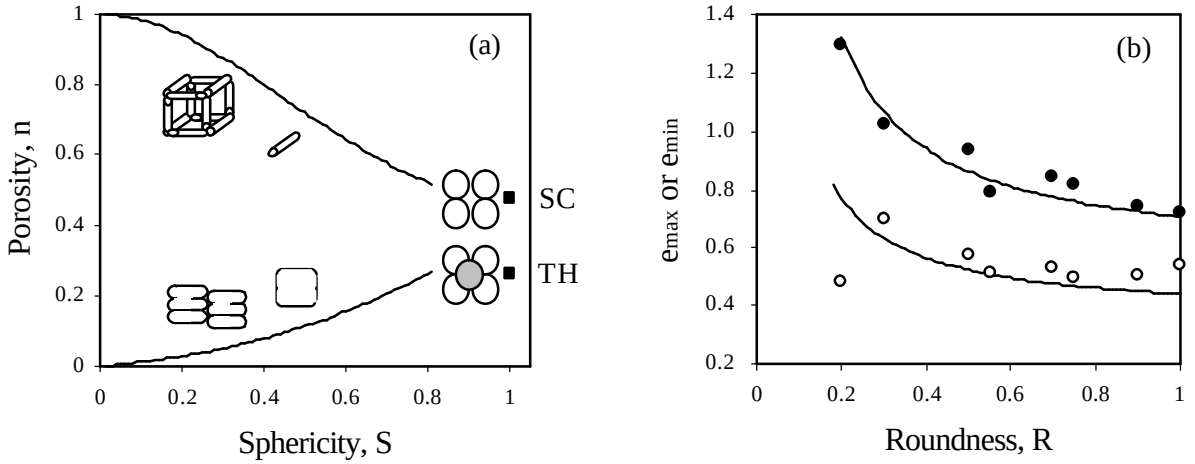


Figure 4. Particle packing and shape. (a) Sphericity. (b) Roundness effects for various uniform sands; trends correspond to Equations 2.

mechanisms combine to affect packing density of micaceous sands. Guimaraes (2002) observed a quasi-linear increase in void ratio with mica content (from e=0.65 at %mica=0, to e~1.1 at %mica=20), when the length of platelets is larger than the diameter of sand grains.

## Stiffness

Different deformation mechanisms are activated at small and large strains. The role of particle shape in each case is analyzed next.

### Small-strain stiffness

During small-strain deformation, the strain level is lower than the elastic threshold strain, interparticle coordination remains constant, and the observed global deformation of the soil is the accumulation of contact level deformations.

The small-strain longitudinal and shear stiffness reflect fabric anisotropy due to aligned *non-spherical platy or ellipsoidal particles*, even under isotropic confinement. Geometric considerations and Hertzian contact behaviour permit exploring the relative magnitude of vertical and horizontal stiffness in horizontally aligned ellipsoids with aspect ratio h/v subjected to an isotropic state of stress (Figure 5). In terms of propagation velocity, the analysis predicts that the horizontal P-wave velocity $V_{P\text{-}hor}$ in horizontally-aligned ellipsoids is greater than the vertical $V_{P\text{-}vert}$. The effect of particle orientation on S-wave velocity anisotropy under isotropic effective stress is explored with two sets of air-dry specimens, one made of mica flakes and a second set prepared with rice grains. Preferential particle alignment

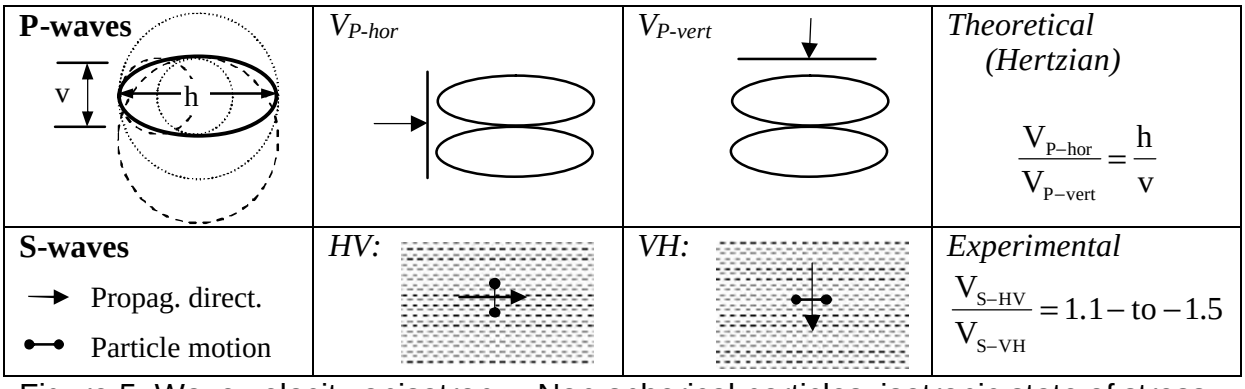


Figure 5. Wave velocity anisotropy - Non-spherical particles, isotropic state of stress

during specimen preparation is readily confirmed in both cases. The specimens are isotropically loaded in a standard triaxial cell, instrumented with bender elements. Effective confinement is varied between 25 and 500 kPa. Experimental results show that the shear wave velocity is higher when the direction of wave propagation is parallel to the main axis of the particles $V_{S\text{-}HV}$, as compared to propagation in specimens where particles are aligned in the direction of particle motion $V_{S\text{-}VH}$. The measured velocity ratio is $V_{S\text{-}HV}/V_{S\text{-}VH}$=1.3-to-1.5 in mica, and $V_{S\text{-}HV}/V_{S\text{-}VH}$= 1.11 in rice (Figure 5).

Mechanical (Hertzian-type) and electrical (Coulombian and DLVO) interactions render the small strain stiffness of soils inherently non-linear and stress-dependent. The shear wave velocity $V_s$ is related to the mean stress on the polarization plane $\sigma_o$' as:

$$V_s = \sqrt{\frac{G}{\rho}} = \alpha\left(\frac{\sigma_0^{'}}{1\text{kPa}}\right)^{\beta} \qquad (3)$$

where $\alpha$=Vs when $\sigma_0$=1kPa, and $\beta$ reflects the sensitivity of $V_s$ to the state of stress. Increased particle angularity (Figure 6-a), roughness (Santamarina and Cascante 1998, Yimsiri and Soga 1999) and platiness (mica-sand mixtures tested in an oedometer instrumented with bender elements - Guimaraes 2002) cause an increase in $\beta$ and a decrease in $\alpha$.

### Oedometric stiffness

Particle deformation at contacts (exacerbated by angularity) and contact slippage (facilitated in smooth particles) determine the deformability of soils under zero-lateral strain $k_o$-loading. Figure 6-b presents compression index values $C_c$ for rounded, natural sands and crushed sands. The bending of platy particles strongly effects $C_c$ as well (Gilboy, 1928; McCarthy and Leonards, 1963).

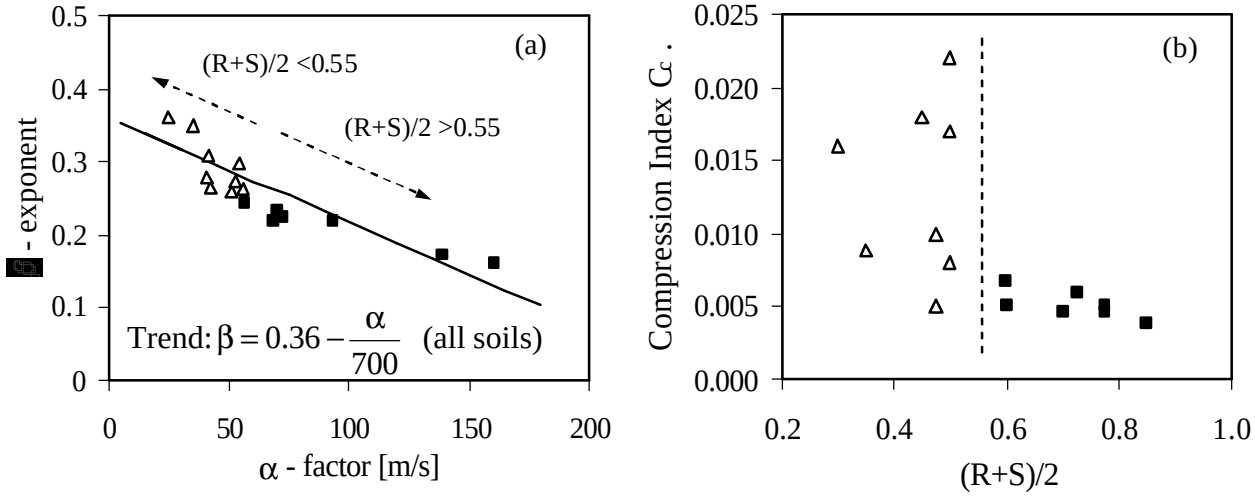


Figure 6. Effect of particle irregularity on small-strain wave propagation velocity and middle-strain oedometric $C_c$. Tests conducted by Dodds (2003) using an oedometer instrumented with bender elements. The $\alpha$-$\beta$ trend is from Santamarina et al. (2001).

## Strength (large strain response)

The deformation of a soil mass at large strains can demand relatively low energy if particles are free to rotate; this is the case when the coordination number is low (i.e., loose packing - Figure 7-a). If the coordination number is high, rotation is frustrated (dense packing). Shear in a rotationally frustrated packing involves either contact slippage or packing dilation to reduce the coordination number. These particle level mechanisms are also responsible for the

evolution of anisotropy during shear. Ultimately, the shear strength of a soil reflects its ability to develop internal force and fabric anisotropy (Rothenburg and Bathurst 1989; Thornton 2000). Within this micromechanical framework, it is appropriate to hypothesize that angularity will add difficulty to particle rotation, roughness will hinder slippage, and both will enhance dilatancy and anisotropy.

## Critical state (shear at constant volume)

The micromechanical analysis of shear deformation suggests and experimental evidence confirms that the constant volume critical state friction angle $\phi_{cv}$ is not just mineral-to-mineral friction, but it depends on particle shape as well. Values of $\phi_{cv}$ measured by the angle of repose are plotted versus *roundness* in Figure 7-b. It is observed that (see also Chan and Page 1997),

$$\phi_{cv} = 42 - 17R \qquad (4)$$

Experimental data for the effect of *roughness* on $\phi_{cv}$ is scarce. Stress-strain trends documented in Santamarina and Cascante (1998) suggest that $\phi_{cv}$ increases with roughness, as hinted by the micromechanical analysis in relation to Figure 7-a.

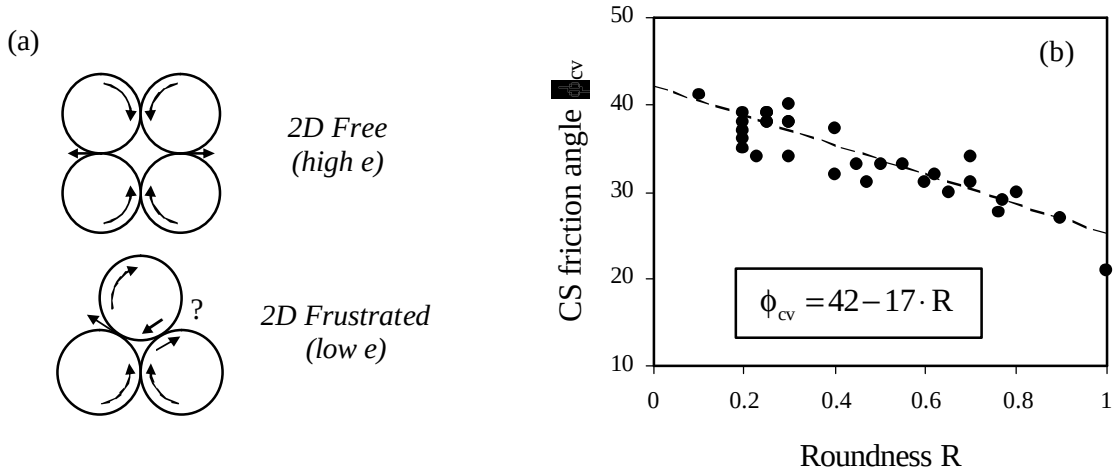


Figure 7. Angularity and roughness affect shear strength. (a) Rotational frustration in dense packing. (b) Constant volume critical state friction angle.

Constant volume critical state shearing is a state of statistical equilibrium between volume reduction due to chain collapse and volume dilation required to reduce interparticle coordination and rotational frustration. Previously published data and new experimental results with angular-crushed and natural-rounded sands show that the critical state void ratio at an effective 100 kPa confinement, $e_{cs100}$, increases with particle irregularity, but remains bounded relative to the extreme void ratios $e_{max}$ and $e_{min}$ (database: 54 specimens),

$$\frac{e_{max} - e_{cs100}}{e_{max} - e_{min}} = 0.3 \pm 0.1 \qquad (5)$$

## Dilation and peak friction angle

Dilation can be an important component of shear strength. As discussed earlier, *angularity and roughness* enhance the dilative tendency of dense packings. The role of particle *sphericity* depends on particle alignment in relation to the shear direction. The local dilatancy of three spherical particles in triangular packing is $\psi$=30°. The triangular packing of three elliptical particles exhibits a local dilation proportional to the particle aspect ratio in the shearing direction $L_N/L_T$ (subindices N and T: lengths in the direction of the normal and shear forces):

$$\tan\psi = \left(\frac{L_N}{L_T}\right)\tan 30 \qquad (6)$$

While local dilation angles can be very high, dilation often occurs concomitantly with strain localization, and much lower values are inferred based on global measurements. High dilation angles around $\psi \approx 30°$ have been measured for locked sands (Dusseault and Morgenstern 1979) and in sands at extremely low confinement (Sture et al. 1998).

Dilation $\psi$ and constant volume friction $\phi_{cv}$ contribute to the measured peak friction angle (Taylor 1948; Bolton 1986):

$$\phi_{max} = \phi_{cv} + 0.8\psi \qquad (7)$$

Therefore, the peak friction angle is also affected by particle irregularity (Holubec and D'Appolonia 1973, Miura et al. 1998).

## Residual friction angle (at particle alignment)

An elliptical particle gains a characteristic alignment between two normally loaded sliding planes, which is related to its slenderness, interfacial friction. Therefore, *non-spherical platy or ellipsoidal particles* both favour the formation of inherent anisotropy and enhance the development of stress-induced fabric anisotropy. The residual strength depends on the fraction of platy particles (must exceed 10-25% by weight) and the mineralogy, i.e., particle thickness or slenderness (Skempton 1964 and 1985; Lupini, Skinner and Vaughan 1981).

## Drained and undrained strength anisotropy

The friction angle varies with the effective stress anisotropy and the intermediate stress captured in the b-coefficient, $b=(\sigma_1-\sigma_2)/(\sigma_1-\sigma_3)$. Typically (Mayne and Holtz 1985; Ladd et al. 1977),

$$\phi_{DSS} > \phi_{AE} \approx 1 \text{ to } 1.5\,\phi_{AC} \qquad (8)$$

Particle shape participates by affecting the evolution of fabric anisotropy, that is, the interplay between chain collapse and the mobilization of interparticle friction in rotational frustration. Lower anisotropy values are observed in bulky coarse particles than in clayey soils.

Undrained strength anisotropy shows an opposite trend, where $S_u(AE) < S_u(AC)$. Examples for sands can be found in Vaid and Sivathayalan (1996), Yoshimine et al. (1999); for silts in Zdravkovic and Jardine (1997); and for clays in Ladd et al. (1977) and Mayne and Holtz (1985). Pore pressure generation is controlled by the buckling of particle chains and the consequent transfer of confinement onto the pore fluid pressure. Buckling vulnerability increases in soils that have been anisotropically consolidated and when subsequent loading reverses the direction of deformation; in this case, the lateral stability of columnar chains is altered. In addition, displacement reversal faces lower skeletal stiffness.

Undrained strength anisotropy also reflects inherent fabric anisotropy in non-spherical particles, and the direction of the loading path relative to particle alignment. Packings sketched in Figure 8 facilitate understanding the pronounced undrained strength anisotropy exhibited by the sand: the granular skeleton is stiffer in AC ($b=0$ $\alpha=0°$) than in AE ($b=1$ $\alpha=90°$), therefore, AE-loading generates more pressure than AC loading.

## Monotonic and cyclic liquefaction

Undrained, AC triaxial test results with uniformly graded rounded Ottawa sand and angular blasting sand suggests that the rounder the sand is the lower the strain at peak strength and at phase transformation (Cho 2001). Numerical DEM cyclic loading simulations with different

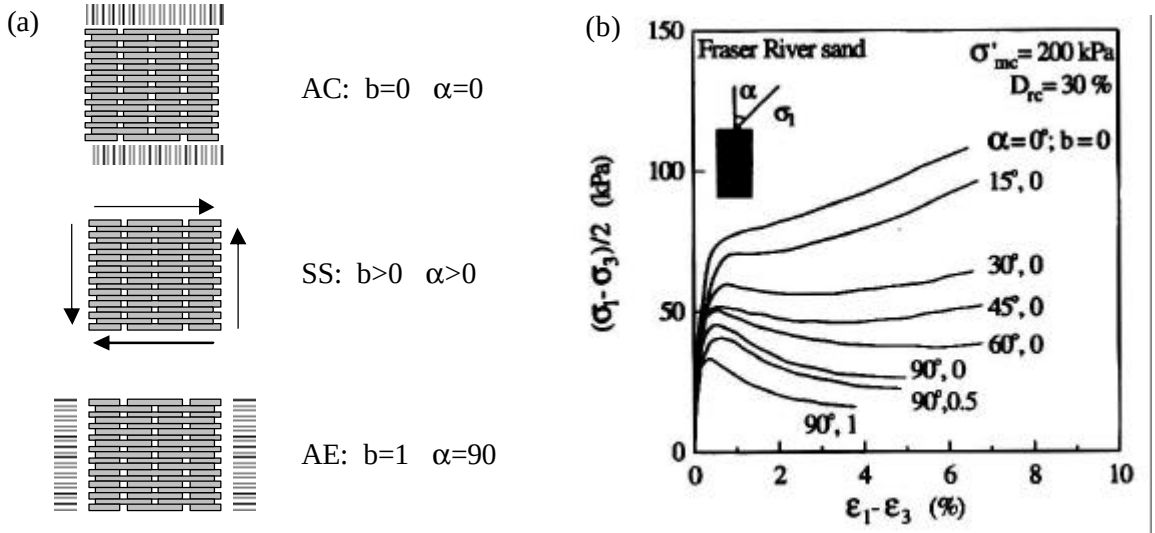


Figure 8. Inherent anisotropy effects on undrained strength. (a) Conceptual model. (b) Data for Fraser river sand (from Vaid and Sivathayalan 1996).

shaped particles show that liquefaction resistance increases with particle irregularity when specimens are prepared at the same void ratio (Ashmawy et al. 2003). This is in agreement with observations made in relation to Equations 2 and 5.

The upwards propagation of the pressure diffusion front created in the liquefied layer after a seismic event can cause the fluidization of shallower strata. Then, the link between Stokes velocity and shape can explain experimental observations that show shape effects on fluidization (Flemmer et al. 1993 - Note: the viscous drag force experienced by a particle in a granular bed is greater than that experience by the same particle in isolation, for the same particle-fluid relative velocity).

### Localization

Elliptical (non-spherical) particles require a higher coordination number than spherical particles to attain stable configuration and particle eccentricity magnifies the mechanical anisotropy of a medium subjected to shear (Oda et al. 1985, Rothenburg and Bathurst 1992). Thus, granular media composed of eccentric (non-spherical) particles are prone to strain localization (or shear band formation), even when the medium exhibits volume contraction during shear (data for rice and mica can be found in Aloufi and Santamarina 1995 and Santamarina and Cho 2003).

## Fluid-related phenomena

The role of particle shape on fluid-related phenomena is often related to the specific surface of the soil mass. Three cases are discussed next.

*Unsaturation - Capillary force*. The capillary force between two parallel platy particles is proportional to the particle area A and independent of the particle thickness t. Yet, the particle mass is proportional to (tA). Therefore, the importance of capillary forces increases with decreasing particle thickness and increasing specific surface (Equation 1). The structure of loess reflects the role of capillary forces on soil formation when small-platy and coarse-bulky particles are involved.

*Conduction and diffusion*. All conduction coefficients in soils depend on particle shape and

specific surface. Examples include hydraulic conductivity (Kozeny-Carman equation - see Endo et al. 2001), and electrical conductivity (the contribution of surface conduction and geometry dependent de-polarization). In addition, anisotropic fabrics of non-spherical particles render conduction properties anisotropic (e.g., Witt and Brauns 1983). Diffusion coefficients are related to conduction coefficients and inherit their particle-shape dependency.

*Filters.* At the microscale of pores, the migration of fine particles (size $d_{fine}$) is prevented if they can form stable bridges at pore throats (size $d_{throat}$) between the larger particles. Experimentally determined $d_{throat}/d_{fine}$ ratios are particle shape dependent. In particular, angular sands bridge more readily than rounded sands (Hall and Harrisberger, 1970).

## Shape sorting - Segregation - Granular flow

Size sorting is ubiquitous in wind and water-transported soils. While the role of shape sorting on soil formation is more subtle, preferential particle shapes can be identified in various stratigraphic regions often due to shape-dependent viscous drag. Industrial applications such as mining and pavement construction often require shape separation.

Most methods designed to separate *coarse-grains* by shape target the differential dynamic response and mobility exhibited by particles of different shape, and they promote displacement on inclined, rotating and/or vibrating planes (Whiteman and Ridway 1988). Sieve-based shape sorting techniques are based on the time it takes a cylinder to traverse a sieve; this time is proportional to $(L/d)^3$ where L is length and d is diameter (Furuuchi and Gotoh 1992). The Stokes terminal settling velocity is smaller for platy, elongated and irregular particles than for spherical particles (the terminal velocity depends on particle orientation, which changes for different Reynold's numbers - Flemmer et al. 1993, Xie and Zhang 2001). Settling time can be used for shape-sorting *fine-grained* soils in the micron-size.

Sorting also takes place in a soil mass subjected to high shear strains. In this case, segregation reflects the different friction coefficients (related to particle mobility). Typical experiments are conducted in rotating cylinders, starting with homogeneous mixtures of particles of different shape (sphericity, angularity or roughness). Results show smooth flow of spherical-smooth particles, intermittent avalanches of rough or angular particles, and the formation of segregated bands of alike particles (Zik et al. 1994, Khosropour et al. 2000).

Several experimental and numerical simulation studies have been conducted to explore the effect of particle shape on granular flow through orifices. Bridging and arching trends are relevant in this context: the more spherical the particle is (as compared to elliptical, platy or cubical), the lower the disruption of flow patterns and the higher the flow rates (Cleary and Sawley 2002 - numerical discrete element models). Two regions are identified: the moving mass and the stagnant mass; the transition zone between these two regions is a low density shear band. The temporary formation of soil arches in the moving mass near the opening causes a decrease in density of the soil beneath it; eventually the arch loses support and collapses. This intermittent, non-linear flow behaviour results in density waves. This behaviour is more prevalent in angular sands than in smooth-spherical sands (Baxter et al. 1989 - experimental, X-ray monitoring).

## Conclusions

Soils are made of grains. Grain size distribution plays a pivotal role in determining soil behaviour. However, particle shape emerges as a significant parameter that needs to be properly characterized and documented as part of every soil characterization exercise.

The three principal scales in particle shape, sphericity, angularity and roughtness, affect soil behaviour. Deviations from smooth spherical shape allow for a wider range in fabric, as denoted by the range between min and max porosities. Ellipticity and platiness (as opposed to *sphericity*) promote inherent anisotropy and affect the evolution of stress-induced anisotropy. Fabric anisotropy affects all types of properties (deformation, strength, conduction, diffusion). Platiness decreases stiffness and residual friction angle. *Angularity and roughness* promote a decrease in small-strain stiffness, an increase in high-strain strength and affect the evolution of stress-induced anisotropy.

Fine grained particles, typically clay minerals, are mostly platy. Particle thickness (relative to double layer thickness) determines specific surface, fabric formation, plasticity and all forms of conduction and diffusion.

## Acknowledgements

SEM pictures in Figure 1 a&b were obtained by A. Palomino. Experimental data invoked in Figure 5 were gathered by B. Sheppard and C-T Yang. Support was provided by NSF, Ga. Mining Industry, and the Smart Infra-Structure Technology Centre SISTeC under KOSEF.

## References

Aloufi, M. and Santamarina, J.C. (1995), Low and High Strain Mechanical Properties of Grain Masses - The Effect of Particle Eccentricity, Trans. ASAE, vol. 38, pp. 877-887.

Ashmawy, A.K., Sukumaran, B., and Vinh Hoang, V. (2003). Evaluating the influence of particke shape on liquefaction behaviour using discrete element modelling, PCW-05.

Barrett, P.J. (1980), The shape of rock particles, a critical review, Sedimentology, vol. 27, pp. 291-303.

Baxter, G.W., Behringer, R.P., Fagert, T. and Johnson, G.A. (1989), Physical Review Letters, vol. 62, pp. 2825-2828.

Bolton, M. D. (1986), The strength and dilatancy of sands, Géotechnique, vol. 36, pp. 65-78.

Bowman, E.T., Soga, K., and Drummnond, W. (2001), Particle shape characterization using Fourier descriptor analysis, Géotechnique, vol. 51, No. 6, pp. 545-554.

Chan, L.C.Y. and Page, N.W. (1997), Particle fractal and load effects on internal friction in powders, Powder Technology, vol. 90, pp. 259-266.

Chen, J.S., Cushman, J.H., and Low, P.F. (1990), Rheological behavior of Na-montmorillonite suspensions, Clays and Clay Minerals, vol. 38, pp. 57-62.

Cho, G.C. (2001), Partially Saturated Particulate Materials and Post Liquefaction Shear Strength, Georgia Institute of Technology, Atlanta, 288 pages.

Clark, N.N., (1987), A new scheme for particle shape characterization based on fractal harmonics and fractal dimensions, Powder Technology, vol. 51, pp. 243-249.

Cleary, P.W. and Sawley M. L. (2002). DEM modelling of industrial granular fows: 3D case studies and the effect of particle shape on hopper discharge, Applied Mathematical Modelling vol. 26, pp. 89–111.

Cubrinovski, M. and Ishihara, K. (2002), Maximum and minimum void ratio characteristics of sands, Soils and Foundation, vol. 42, No. 6, pp. 65-78.

Dodds, J.S. (2003), Crushed stone - Shape effects, MSc Thesis, Georgia Institute of Technology, Atlanta, 175 pages.

Endo, Y., Chen, D.-R., and Pui, D.Y.H. (2001), Air and water permeation resistance across dust cakes on filters, Powder Technology, vol. 118, pp. 24-31.

Flemmer, R.L.C., Pickett, J. and Clark, N.N. (1993), An experimental study on the effect of particle shape on fluidization behaviour, Powder Technology, vol. 77, pp. 123-133.

Folk, R.L. (1955), Student operator error in determination of roundness, sphericity, and grain size, Journal of Sedimentary Petrology, vol. 25, No. 4, pp. 297-301.

Fraser, H.J. (1935), Experimental study of the porosity and permeability of clastic sediments, Journal of Geology, vol. 13, No. 8, Part 1, pp. 910-1010.

Furuuchi, M. and Gotoh, K. (1992), Shape separation of particles, Powder Tech., pp. 1-9.

Gilboy, G. (1928), The compressibility of sand-mica mixtures, Proc. American Society of Civil Engineering, vol. 54, pp. 555-568.

Guimaraes, M. (2002), Crushed stone fines and ion removal from clay slurries - fundamental studies, PhD thesis, Georgia Institute of Technology, Atlanta, 238 pages.

Hall, C.D. and Harrisberger, W.H. (1970), Stability of Sand Arches: A Key to Sand Control, SPE Society of Petroleum Engineers Journal, Vol. 21, No. 2, pp. 236-248.

Holubec I. and D'Appolonia E. (1973), Effect of particle shape on the engineering properties of granular soils, ASTM STP 523, pp. 304-318.

Hyslip, J.P. and Vallejo, L.E. (1997), Fractal analysis of the roughness and size distribution of granular materials, Engineering Geology, vol. 48, pp. 231-244.

Khosropour, R., Valachovic, E. and Lincoln, B. (2000). Flow and pattern formation in a binary mixture of rotating granular materials, Physical Review E, vol. 62, pp. 807-812.

Krumbein, W.C. (1941), Measurement and geological significance of shape and roundness of sedimentary particles, Journal of Sedimentary Petrology, vol. 11, No. 2, pp. 64-72.

Krumbein, W.C. and Sloss, L.L. (1963), Stratigraphy and Sedimentation, Second Edition, W.H. Freeman and Company, San Francisco, p. 660.

Kuenen, P.H. (1960). Experimental abrasion 4: eolian action. J.Geology, vol. 68, pp. 427-449.

Ladd, C. C., Foott, R., Ishihara, K., Schlosser, F. and Poulos, H. G. (1977), Stress-deformation and strength characteristics, Proc. 9th ICSMFE, vol. 2, Tokyo, pp. 421-494.

Li, D.Y. and Chen, L.Q. (1999), Shape evolution and splitting of coherent particles under applied stresses, Acta Metallurgica, vol. 47, pp. 247-257.

Lupini, J. F., Skinner, A. E. and Vaughan, P. R. (1981), The drained residual strength of cohesive soils, Géotechnique, vol. 31, pp. 181-213.

McCarthy, D.F. and Leonards, R.J. (1963), Compaction and compression characteristics of micaceous fine sands and silts, Highway Research Record, vol. 22, pp. 22-27.

Margolis, S.V. and Krinsley, D.H. (1974), Processes of formation and environmental occurrence of microfeatures on detrital quartz grains, Am. J. Sc., vol . 274, pp. 449-464.

Mayne, P.W. and Holtz, R.D. (1985), Effect of principal stress rotation on clay strength, Proc. 11th ICSMFE, San Francisco, vol. 2, pp 579-582.

Meloy, T.P. (1977), Fast Fourier transforms applied to shape analysis of particle silhouettes to obtain morphological data, Powder Technology, vol. 17, pp. 27-35.

Miura, K., Maeda K., Furukawa, M., Toki, S. (1998) Mechanical characteristics of sands with different primary properties, Soils and Foundations, vol. 38, pp. 159-172.

Nabarro, F.R.N. (1940), The strains produced by precipitation in alloys, Proc. Royal Soc. of London, vol. 175, no. 963, pp. 519-538.

Noh, D.S., Koh, Y., and Kang I.S. (1998), Numerical solutions for shape evolution of a particle growing in axisymmetric flows of supersaturated solution, J. Crystal Growth, vol. 183, pp. 427 440.

Oda, M., Nemat-Nasser, S. and Konishi, J. (1985), Stress-induced anisotropy in granular masses, Soils and Foundation, vol. 25, pp. 85-97.

Powers, M.C. (1953), A new roundness scale for sedimentary particles, Journal of Sedimentary Petrology, vol. 23, No. 2, pp. 117-119.

Pusch, R. (1970), Microstructural changes in soft quick clay at failure, Canadian Geotechnical Journal, vol. 7, p. 1-7.

Rahaman, M.N. (1995), Ceramic Processing and Sintering, Dekker Inc., NY, 770 pages.

Rand, B., Pekenc, E., Goodwin, J.W., and Smith, R.W. (1980), Investigation into the

existence of edge-face coagulated structures in Na-montmorillonite suspensions, Journal of the Chemical Society, Faraday Transaction I, vol. 76, pp. 225-235.

Rothenburg, L. (1993), Effects of particle shape and creep in contacts on micromechanical behavior of simulated sintered granular media, Mechanics of Granular Materials and Powder Systems, vol. 37, pp. 133-142.

Rothenburg, L. and Bathurst, R. J. (1989), Analytical study of induced anisotropy in idealized granular material, Géotechnique, vol. 49, pp. 601-614.

Rothenburg, L. and Bathurst, R.J. (1992), Micromechanical features of granular assemblies with planar elliptical particles, Géotechnique, vol. 42, pp. 79-95.

Santamarina, J.C. and Cascante, G. (1998), Effect of Surface Roughness on Wave Propagation Parameters, Geotechnique, vol. 48, no. 1, pp. 129-137.

Santamarina, J.C., Klein, K. and Fam, M. (2001). Soils and Waves, J. Wiley and Sons, Chichester, UK, 488 pages.

Santamarina, J.C. and Cho, G.C. (2003), The Omnipresence of Localization in Geomaterials, Deformation Characteristics of Geomaterials, Lyon.

Shimobe, S., and Moroto, N. (1995), A new classification chart for sand liquefaction, Earthquake Geotechnical Engineering, K. Ishihara (ed.), Balkema, pp. 315-320.

Skempton, A.W. (1964), Long-term stability of clay slopes, Géotechnique, pp. 77-102.

Skempton, A. W. (1985), Residual strength of clays in landslides, folded strata and the laboratory, Géotechnique, vol. 35, pp. 3-18.

Smalley, I.J. (1966), Formation of quartz sand, Nature 211, pp. 173-174.

Sture, S., Costes, N. C., Batiste, S. N., Lankton, M. R., AlShibli, K. A., Jeremic, B., Swanson, R. A. and Frank, M. (1998), Mechanics of granular materials at low effective stresses, ASCE Journal of Aerospace Engineering, vol. 11, pp. 67-72.

Taylor, D. W. (1948), Fundamentals of Soil Mechanics, Wiley, New York, 699 pages.

Thornton, C. (2000), Numerical Simulations of Deviatoric Shear Deformation of Granular Media, Geotechnique, vol. 50, pp. 43-53.

Vaid, Y.P. and Sivathayalan, S. (1996), Static and Cyclic Liquefaction Potential of Fraser Delta Sand in Simple Shear and Triaxial Tests, Canadian Geotech J., vol. 33, pp. 281-289.

Wadel, H. (1932), Volume, shape, and roundness of rock particles, Journal of Geology, vol. 40, pp. 443-451.

Whiteman, A. and Ridway, K. (1988). A comparison between two methods of shape-sorting particles. Powder Technology, vol. 56, pp. 83-94.

Witt, K.-J., and Brauns, J. (1983), Permeability-anisotropy due to particle shape, Journal of Geotechnical Engineering, vol. 109, No. 9, pp. 1181-1187.

Xie, H.-Y. and Zhang, D.-W. (2001), Stokes shape factor and its application in the measurement of spherity of non-spherical particles, Powder Tech., vol. 114, pp. 102-105.

Yimsiri, S., Soga, K. (1999), Effect of surface roughness on small-strain modulus: micromechanics view. Pre-failure Deformation Characteristics of Geomaterials: Proceedings, 2nd International Symposium, Torino, Italy; Edited by M. Jamiolkowski, R. Lancellotta, D. Lo Presti, 597-602.

Yoshimine, M., Robertson, P.K. and Wride, C.E. (1999), Undrained Shear Strength of Clean Sands to Trigger Flow Liquefaction, Canadian Geotechnical J., vol. 36, pp. 891-906.

Youd, T.L. (1973), Factors controlling maximum and minimum densities of sands, Evaluation of Relative Density and Its Role in Geotechnical Projects Involving Cohesionless Soils, ASTM STP 523, pp.98-112.

Zdravkovic, L. and Jardine, R.J. (1997), Some Anisotropic Stiffness Characteristics of a Silt Under General Stress Conditions, Géotechnique, vol. 47, no. 3, pp. 407-437.

Zik, O., Levine, D., Lipson, S.G., Shtrikman, S. and Stavans, J. (1994), Rotationally induced segretation of granular materials, Physical Review letters, vol. 73, pp. 644-647.